# Interleukin-6 Reduces β-Cell Oxidative Stress by Linking Autophagy With the Antioxidant Response

Michelle R. Marasco,[1] Abass M. Conteh,[2] Christopher A. Reissaus,[1] John E. Cupit V,[1] Evan M. Appleman,[1] Raghavendra G. Mirmira,[1,2,3,4] and Amelia K. Linnemann[1,2,3,4]

*Diabetes 2018;67:1576–1588 | https://doi.org/10.2337/db17-1280*

**Production of reactive oxygen species (ROS) is a key instigator of β-cell dysfunction in diabetes. The pleiotropic cytokine interleukin 6 (IL-6) has previously been linked to β-cell autophagy but has not been studied in the context of β-cell antioxidant response. We used a combination of animal models of diabetes and analysis of cultured human islets and rodent β-cells to study how IL-6 influences antioxidant response. We show that IL-6 couples autophagy to antioxidant response and thereby reduces ROS in β-cells and human islets. β-Cell-specific loss of IL-6 signaling in vivo renders mice more susceptible to oxidative damage and cell death through the selective β-cell toxins streptozotocin and alloxan. IL-6-driven ROS reduction is associated with an increase in the master antioxidant factor NRF2, which rapidly translocates to the mitochondria to decrease mitochondrial activity and stimulate mitophagy. IL-6 also initiates a robust transient decrease in cellular cAMP levels, likely contributing to the stimulation of mitophagy to mitigate ROS. Our findings suggest that coupling autophagy to antioxidant response in β-cells leads to stress adaptation that can reduce cellular apoptosis. These findings have implications for β-cell survival under diabetogenic conditions and present novel targets for therapeutic intervention.**

All forms of diabetes result from either dysfunction and/or death of islet β-cells, and increasing evidence has implicated the generation of reactive oxygen species (ROS) in this process (1). The typical response to increased production of ROS includes activation of the master transcriptional regulator NRF2, which in turn activates a host of antioxidant genes and thus plays a critical role in protection against ROS-mediated injury (2). An inadequate response to ROS leads to uncontrolled oxidative stress and subsequent cell death. Thus, a maladaptive response to ROS likely plays a significant role in diabetes pathogenesis (3), and the activation of antioxidant pathways in the face of increased ROS may be key to β-cell survival.

Multiple links between antioxidant response and autophagy have been demonstrated recently (4). It is important to note that evidence shows that stimulation of the autophagy machinery leads to activation of NRF2 (5), whereas β-cell-specific loss of NRF2 leads to increased sensitivity to oxidative stress (6). Autophagy, as an adaptive response to cellular stress, has been shown to promote survival (7) and plays a critical role in antioxidant response in degenerative diseases (8). In addition, autophagy is crucial to β-cell function and homeostasis (9). These observations suggest that activation of islet autophagy may bolster antioxidant response, leading to reduced oxidative stress and thereby reduced apoptosis.

One potential endocrine target in islet response to ROS is the pleiotropic cytokine interleukin (IL) 6, which we recently found to stimulate β-cell autophagy both in vitro and in vivo and to protect β-cells from apoptosis (10). It is interesting to note that the IL-6 promoter contains an antioxidant response element and NRF2 can stimulate its expression (11), implying regulatory links between the signaling pathways. The link between IL-6-mediated stimulation of β-cell autophagy and ROS mitigation has not been tested. Here we show that IL-6 rapidly activates

[1]Department of Pediatrics, Indiana University School of Medicine, Indianapolis, IN
[2]Department of Biochemistry and Molecular Biology, Indiana University School of Medicine, Indianapolis, IN
[3]Department of Cellular and Integrative Physiology, Indiana University School of Medicine, Indianapolis, IN
[4]Center for Diabetes and Metabolic Diseases, Indiana University School of Medicine, Indianapolis, IN

Corresponding author: Amelia K. Linnemann, aklinnem@iu.edu.

Received 23 October 2017 and accepted 7 May 2018.

This article contains Supplementary Data online at http://diabetes.diabetesjournals.org/lookup/suppl/doi:10.2337/db17-1280/-/DC1.

a cascade of events that leads to a reduction of proinflammatory cytokine–induced ROS generation in both cultured β-cells and human islets. Loss-of-function studies in vivo further demonstrate that IL-6 signaling in β-cells plays a key role in the response to ROS that are generated by the toxic glucose analogs streptozotocin (STZ) and alloxan. We show that acute upregulation of signaling events by IL-6 in β-cells orchestrates activation of autophagy and antioxidant response to collectively reduce ROS and promote survival under diabetogenic conditions.

## RESEARCH DESIGN AND METHODS

### Cell and Islet Culture

INS1 (832/13) cells (a gift from Dr. C. Newgard, Duke University) were cultured in RPMI 1640 medium (11 mmol/L glucose) supplemented with 10 mmol/L HEPES, 2 mmol/L glutamine, 1 mmol/L sodium pyruvate, 50 μmol/L β-mercaptoethanol, 10% FBS, and 1% antibiotic/antimycotic. Human islets were obtained through the Integrated Islet Distribution Program and cultured in suspension in islet medium (5.8 mmol/L glucose; Prodo Laboratories, Inc.) containing 5% Human AB Serum (Prodo Laboratories, Inc.), 1% glutamine/glutathione supplement (Prodo Laboratories, Inc.), and 10 μg/mL ciprofloxacin (Fisher Scientific). Cells and islets were treated for 24 h with 200 ng/mL IL-6 or with a proinflammatory cytokine cocktail comprising 100 ng/mL interferon (IFN)-γ, 50 ng/mL tumor necrosis factor-α (TNF-α), and 10 ng/mL IL-1β. For combined treatment, cells and islets were pretreated with IL-6 for 4 h prior to addition of the cytokine cocktail. Mouse and human IL-6 were from Miltenyi Biotec; mouse TNF-α, IL-1β, and IFN-γ were from ProSpec. Human TNF-α, IL-1β, and IFN-γ were from R&D Systems. Rat Nfe2l2 small interfering RNA (siRNA, L-080047-02-0005) and pooled, nontargeting control siRNA (D-001810-10-05) were purchased from Dharmacon, Inc. All transfections were done using Lipofectamine 2000 (Invitrogen).

### In Vitro Oxidative Stress Measurements

To analyze oxidative stress, treated cells were incubated with 1 μmol/L CellROX Deep Red Reagent (Thermo Fisher Scientific) at 37°C for 30 min, then stained with Hoescht (Thermo Fisher Scientific) for 15 min. Cells were washed and imaged in RPMI 1640 medium lacking phenol red. Islets were incubated with 5 μmol/L CellROX Deep Red Reagent (Thermo Fisher Scientific) at 37°C for 30 min, then stained with Hoescht (Thermo Fisher Scientific) for 15 min and fixed with 3.7% paraformaldehyde for 20 min at room temperature. Samples were imaged on a Zeiss LSM 700 laser scanning confocal microscope.

### Generation of β-Cell-Specific IL-6Rα Knockout Mice

Mice containing LoxP sites surrounding exons 4–6 of the *Il6ra* gene were purchased from The Jackson Laboratory (stock no. 012944). Because mice were bred on a mixed C57BL/6J/6N background, they were backcrossed to C57BL/6J wild-type mice (stock no. 002650; The Jackson Laboratory) to generate *IL6rα* floxed mice on a pure C57BL/6J background. Floxed mice were then bred with B6(Cg)-*Ins1*$^{tm1.1(cre)Thor}$/J mice (stock no. 026801; The Jackson Laboratory) to create β-cell-specific IL-6 receptor knockout mice. Mice were housed in a temperature-controlled facility with a 12-h light/12-h dark cycle and were given free access to food and water unless indicated otherwise for specific experiments. All experiments were approved by the Indiana University School of Medicine Institutional Animal Care and Use Committee.

Islets from control and knockout mice were isolated following collagenase perfusion of pancreata, as previously described (12). For flow sorting, islets were dispersed with Accutase (STEMCELL Technologies Inc.) and incubated with Newport Green DCF Diacetate (Thermo Fisher Scientific) for 30 min, followed by fluorescence-activated cell sorting of populations with high and low Newport Green positivity (13).

### STZ and Alloxan Treatments

For STZ treatments, 8-week-old mice with the indicated genotypes were injected intraperitoneally with 45 mg/kg STZ (S0130; Sigma-Aldrich) in 300 μL saline daily for five consecutive days. Solutions were prepared immediately before injection. Control injections consisted of equal volumes of saline on the same days. On days 8, 15, and 30 (i.e., 3, 10, and 25 days after the final injection), mice deprived of food overnight were given glucose tolerance tests. In brief, animals were given intraperitoneal injections of 2 g/kg glucose (in saline); dosing was based on total body mass. Blood glucose was measured with an AlphaTRAK 2 glucometer (Abbott) before glucose injection and 5, 15, 30, 60, 90, and 120 min after injection. To analyze early response to STZ, one cohort of mice comprised of control or *IL6rα* knockout mice injected with either saline or STZ (three mice per condition) were euthanized on day 9 by cervical dislocation, and tissue was collected for analysis. To assess the development of hyperglycemia, the blood glucose levels of an additional cohort of mice fed randomly were monitored every other day until day 26. The development of diabetes was characterized as two consecutive blood glucose readings over 250 mg/dL. Mice were euthanized by cervical dislocation after the glucose tolerance test (GTT) on day 30, and tissue was collected for analysis.

For alloxan treatments, mice were fasted overnight before injection of 150 mg/kg alloxan monohydrate (A7413; Sigma-Aldrich) in 300 μL saline mixed immediately before injection. Control injections consisted of equal volumes of saline. After receiving the injections, mice were given free access to food and water for the duration of the experiment. To analyze early response to alloxan, one cohort of mice comprised of control or *IL6rα* knockout mice injected with either saline or alloxan (three mice per condition) were euthanized by cervical dislocation 6 h after injection, and tissue was collected. Serum insulin was measured using a STELLUX Chemiluminescent Rodent Insulin

ELISA (ALPCO), according to the manufacturer's instructions. Blood glucose was measured as described above for STZ. To assess the development of hyperglycemia in response to alloxan injection, an additional cohort of mice was monitored daily until day 5. These mice were then overnight fasted on day 7 and were given GTTs on day 8 (using intraperitoneal injections of 0.5 g/kg glucose in saline). Mice were euthanized by cervical dislocation after the GTTs and tissues were collected.

### INS-1 and Mouse Islet Live-Cell Imaging

To image mitochondrial membrane potential, INS-1 cells were incubated with tetramethylrhodamine methyl-ester (TMRM) (100 nmol/L; Thermo Fisher Scientific) and MitoTracker Green (200 nmol/L; Thermo Fisher Scientific) for 30 min before IL-6 stimulation in phenol-free media. To image autophagy stimulated by IL-6, INS-1 cells were transfected with pBABE-puro mCherry–enhanced green fluorescent protein–light chain (LC) 3B (plasmid 22418; Addgene) (14). To analyze cAMP dynamics, isolated mouse islets were transfected with an mNeon cADDis cAMP biosensor (Montana Molecular). Islets were imaged in a Krebs-Ringer bicarbonate solution with 20 mmol/L HEPES and 16.7 mmol/L glucose. Islets were treated with exendin-4 (100 nmol/L), IL-6 (200 ng/mL), and isoproterenol (1 μmol/L). Live-cell imaging was performed using a Nikon TiE spinning disk confocal microscope equipped with a $CO_2$-controlled 37° stage. Images were processed and quantified using ImageJ and CellProfiler software.

### Immunostaining

Cells grown on coverslips were fixed with 3.7% paraformaldehyde and immunostained according to the method described by Linnemann et al. (10). Alternatively, freshly isolated pancreata were fixed with 3.7% paraformaldehyde for 3 h then transferred to 70% ethanol before being embedded in paraffin. Antigens were retrieved from 5-μm sections using a citrate-based antigen unmasking solution (Vector Laboratories). Samples were blocked with Dako blocking solution, then incubated overnight with primary antibodies in Dako antibody diluent. To analyze immunofluorescence, slides were incubated with fluorescence-conjugated secondary antibodies and DAPI (Thermo Fisher Scientific) in antibody diluent, then mounted with VECTASHIELD mounting medium (Vector Laboratories). Images were collected on a Zeiss LSM 700 laser scanning confocal microscope for standard confocal microscopy or a Zeiss ELYRA superresolution microscope for structured illumination microscopy (used for colocalization studies). To measure β-cell mass, tissue sections were stained as described previously (15), then mounted with Permount mounting medium (Thermo Fisher Scientific) and scanned using a Zeiss Axio Scan imager.

### Cell Fractionation and Western Blotting

INS-1 cells treated with vehicle or 200 ng/mL IL-6 were lysed in fractionation buffer (20 mmol/L Hepes [pH 7.4], 10 mmol/L KCl, 2 mmol/L $MgCl_2$, 1 mmol/L EDTA, 1 mmol/L dithiothreitol, and phosphatase/protease inhibitors). Nuclei and mitochondria were separated sequentially from cytoplasm by centrifugation, then lysed in Tris-buffered saline with 0.1% SDS. Proteins were resolved using 4–20% SDS-PAGE gels (Bio-Rad Laboratories, Inc.) and transferred to polyvinylidene difluoride membranes (EMD Millipore). Membranes were blocked with Odyssey Blocking buffer (LI-COR) then probed overnight at 4°C with primary antibodies in Tris-buffered saline containing 0.1% Tween-20 and 5% BSA. Membranes then were incubated with IRdye conjugated secondary antibodies (LI-COR) and imaged on an Odyssey imager (LI-COR). All antibodies and dilutions used are listed in Supplementary Table 1.

### Statistical Analysis

All experiments were performed at least in biological triplicate. For Western blot and immunofluorescence data, representative images are shown in all figures. Data are presented as the mean ± SEM. *P* values were calculated in GraphPad Prism software using one-way ANOVA with multiple comparisons or the unpaired Student *t* test, as appropriate. To analyze pancreas immunostaining, at least 10 independent islets were analyzed in at least two nonconsecutive tissue sections from each mouse. Fluorescence intensity was quantified using ImageJ, CellProfiler, and Zen software (Zeiss). To analyze β-cell mass, sections were analyzed from three independent locations spaced evenly throughout each pancreas. Islet and pancreas areas were measured using Zen software (Zeiss).

## RESULTS

### IL-6 Reduces ROS Through Direct Action on β-Cells

We previously found that IL-6 was able to protect INS-1 β-cells from proinflammatory cytokine–induced apoptosis. Because proinflammatory cytokines stimulate ROS buildup in islets (16), we wanted to determine whether IL-6 played a role in preventing or reducing the ROS generated under these conditions. We found that in both INS-1 β-cells (Fig. 1*A*) and whole human islets (Fig. 1*B*), treatment with IL-6 reduces the ROS buildup generated by proinflammatory cytokines.

### Loss of the β-Cell IL-6 Receptor Renders Mice More Susceptible to STZ-Induced Oxidative Damage and Development of Diabetes

To determine whether the β-cell IL-6 receptor mediates IL-6-driven ROS reduction, we generated pancreatic β-cell-specific IL-6 receptor knockout ($IL6R\alpha^{\Delta\beta}$) mice. Flow-sorted β-cells from islets isolated from these mice had significantly reduced expression of the *Il6ra* gene (more than a ninefold reduction), whereas expression of *Gp130*, the common component of the IL-6 receptor family, was unaffected (Fig. 2*A*). No effect on insulin gene expression was observed in knockout islets (Supplementary Fig. 1). Intact isolated islets also had reduced STAT3 activation in response to exogenous IL-6 treatment (Fig. 2*B*).

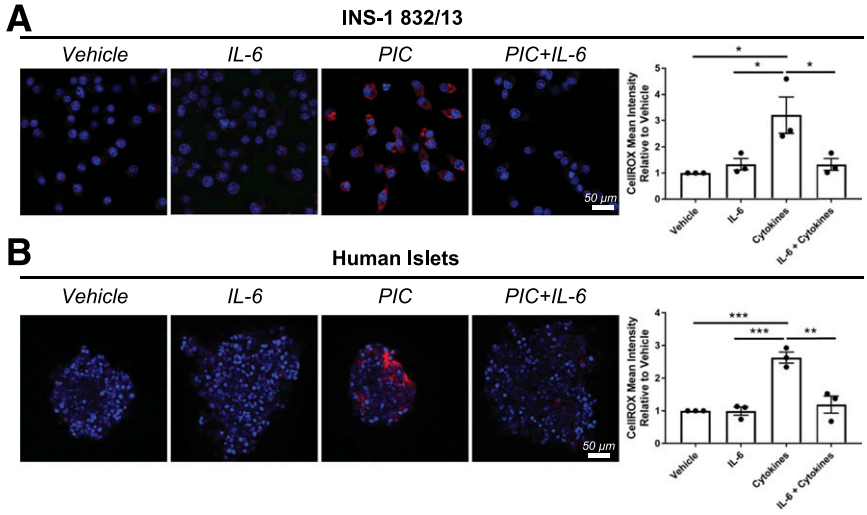


**Figure 1**—IL-6 reduces the amount of ROS generated by proinflammatory cytokines. INS-1 cells (*A*) and human islets (*B*) were treated for 24 h with vehicle; 200 ng/mL recombinant mouse IL-6; a proinflammatory cytokine cocktail (PIC) consisting of 100 ng/mL IFN-γ, 50 ng/mL TNF-α, and 10 ng/mL IL-1β; or the combination of PIC and IL-6. ROS accumulation was measured using the fluorescent dye CellROX Deep Red. Nuclei were stained with DAPI (blue). Graphs show the quantification of the mean CellROX fluorescence intensity for each condition relative to vehicle. Data are mean ± SEM for 3 individual experiments. $^{*}P < 0.05$; $^{**}P < 0.01$; $^{***}P < 0.001$.

IL6Rα$^{Δβ}$ mice exhibited weight gain and glucose tolerance that were indistinguishable from those in control littermates (Fig. 2*C* and *D*).

To test whether islets from IL6Rα$^{Δβ}$ mice are more susceptible in vivo to ROS-induced β-cell death, we used a model of diabetes induced by multiple low doses of STZ

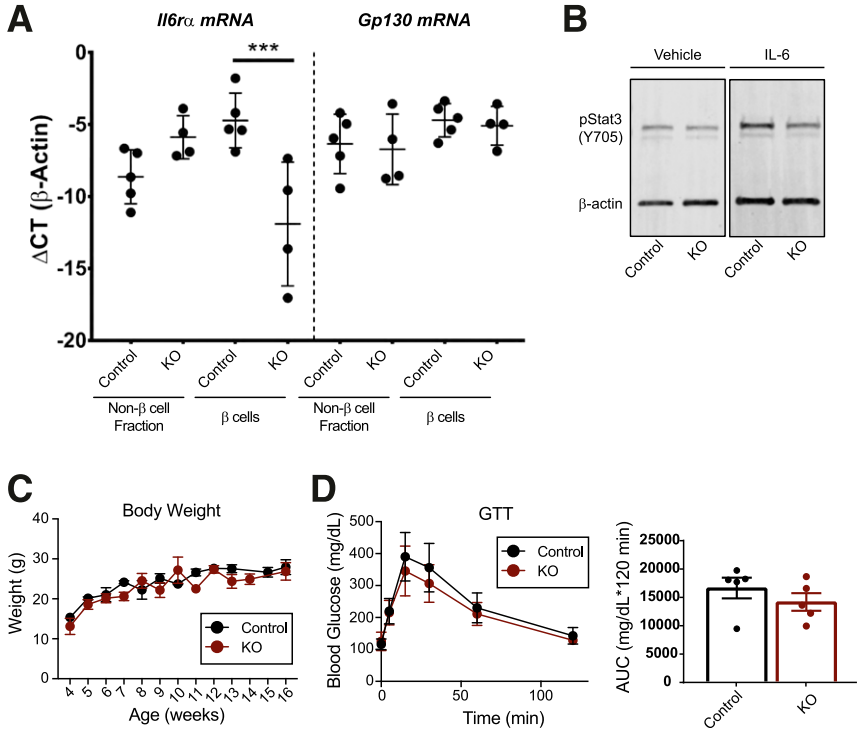


**Figure 2**—Characterization of β-cell-specific IL-6Rα knockout (KO) mice. *A*: *Il6rα* and *gp130* expression were measured in flow-sorted β-cells and in the non-β-cell fractions (i.e., cells that were not sorted by high Newport Green positivity) from knockout mice and littermate controls. *B*: Representative Western blotting shows STAT3 phosphorylation at tyrosine 705 in islets from IL-6Rα KO and littermate control mice treated with vehicle or IL-6. *C*: Body weight measurements of IL-6Rα KO mice and control littermates between 4 and 16 weeks of age. *D*: Results of GTTs in IL-6Rα KO mice and littermate controls at 12 weeks of age (left panel); the area under the curve (AUC) is shown in the right panel. Data are mean ± SEM for 3–5 individual mice. $^{***}P < 0.001$. ΔCT, difference in threshold cycle between the gene expression of a sample of interest versus a control sample; pStat3, phosphorylated Stat3.

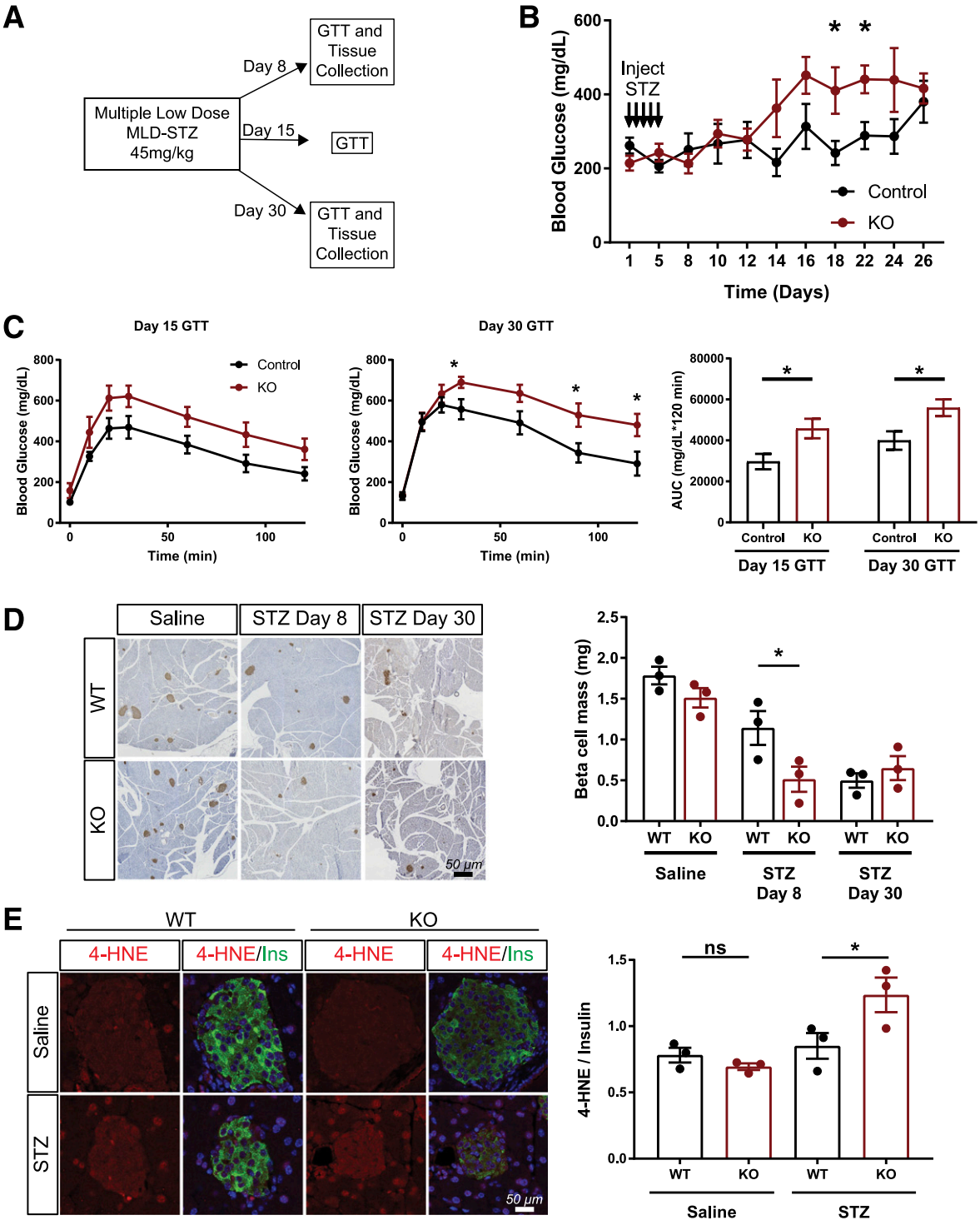


**Figure 3—**IL-6Rα$^{\Delta\beta}$ mice are more susceptible to STZ-induced β-cell oxidative stress and apoptosis. *A*: Design of experiments applying multiple low-dose (MLD) STZ treatments. *B*: Blood glucose levels in mice fed randomly were monitored every other day for 26 days after the first STZ injection. Black arrows indicate days of STZ injection (first 5 days). *C*: Graphs show the results of GTTs performed on days 15 and 30 (left and middle panels), and the areas under the curve (AUC) (right panel). *D*: Representative images of pancreata (left), collected either at day 8 or day 30 after first STZ injection, from which β-cell mass was calculated ( insulin staining appears brown), and quantification of β-cell mass (right). *E*: Representative images of pancreata from STZ day 8 (left), immunostained for insulin (Ins; green) and 4-HNE (red); nuclei were stained with DAPI (blue). The graph to the right shows quantification of 4-HNE relative to remaining insulin. Quantification of 4-HNE and insulin levels individually is shown in Supplementary Fig. 2*B* and *C*. Data are mean ± SEM for 3–5 individual mice. *$P < 0.05$. KO, knockout; ns, not significant; WT, wild type.

(Fig. 3*A*), which generates β-cell ROS and DNA damage that lead to apoptosis (17–19). To determine whether loss of IL-6 signaling makes β-cells more susceptible to oxidative stress, we analyzed a cohort of STZ-injected animals before extensive β-cell death and development of overt diabetes. Blood glucose and glucose tolerance were monitored over time in a second cohort of mice. IL6Rα$^{\Delta\beta}$ mice developed hyperglycemia in response to STZ faster than did control mice (Fig. 3*B*), and we observed a trend toward earlier development of diabetes, with no change in weight (Supplementary Fig. 2*A* and *B*). STZ-treated knockout mice were, however, more glucose intolerant at both day 15 and day 30 (Fig. 3*C*), but not at day 8, before the development of hyperglycemia (Supplementary Fig. 2*C*). STZ treatment resulted in significantly decreased β-cell mass in both wild-type and knockout mice relative to saline-injected mice (Fig. 3*D*). However, consistent with our observation of the development of exacerbated glucose intolerance, IL6Rα$^{\Delta\beta}$ mice had a significantly greater loss of β-cell mass when measured early in response to STZ treatment, suggesting that IL-6 signaling in β-cells protects against STZ-induced apoptosis (Fig. 3*D*). At this early time point, STZ-treated knockout mice displayed evidence of greater oxidative stress in islets, as shown by increased 4-hydroxynononeal (4-HNE) staining, relative to that in STZ-treated wild-type mice (Fig. 3*E*). Because knockout mice had significantly reduced β-cell mass, islet oxidative stress was quantified as a function of insulin remaining in each islet (individual values are shown in Supplementary Fig. 2*D* and *E*).

### Loss of the β-Cell IL-6 Receptor Renders Mice More Susceptible to Alloxan-Induced Oxidative Damage

To assess further whether IL6Rα$^{\Delta\beta}$ mice are more susceptible to ROS buildup, we treated wild-type and knockout mice with alloxan, which produces ROS as direct metabolites (18,19). To assess early responses to alloxan treatment, tissues from some mice were analyzed 6 h after injection, at the peak of ROS production, before widespread β-cell death (18), whereas a second cohort was followed for 8 days to assess diabetes development (Fig. 4*A*). We did not observe significant differences in the blood glucose levels of randomly fed IL6Rα$^{\Delta\beta}$ mice relative to controls (Fig. 4*B*), nor in the day 8 GTT results or body weight (Supplementary Fig. 3*A* and *B*). However, consistent with the previous observation that alloxan induces a characteristic increase in circulating insulin due to β-cell degranulation and cell membrane rupture (18), alloxan-injected IL6Rα$^{\Delta\beta}$ mice had significantly increased circulating insulin 6 h after injection (Fig. 4*C*). In a similar way, while we did not observe differences in β-cell mass at the early or later time point (Fig. 4*D*), 4-HNE levels were significantly increased in alloxan-injected IL6Rα$^{\Delta\beta}$ mice (Fig. 4*E*), indicating early increases in oxidative damage to islets. These data suggest that loss of β-cell IL-6 receptor signaling renders islets more susceptible to in vivo alloxan-induced oxidative damage.

### IL-6 Stimulates the Master Antioxidant Response Factor NRF2 to Reduce ROS

Antioxidant response is primarily controlled through rapid action of the transcription factor NRF2, which activates a network of immediate-early genes involved in ROS mitigation (20). We found that IL-6 stimulates rapid accumulation of NRF2 protein within 5 min of treatment in both INS-1 β-cells (Fig. 5*A*) and human islets (Fig. 5*B*). This accumulation of NRF2 is followed by a reduction in levels of the NRF2 inhibitor KEAP1 within 15 min of treatment of INS-1 cells with IL-6 (Fig. 5*A*).

In the cytoplasm, KEAP1 binds to NRF2 and targets it for degradation by the proteasome. Disruption of the interaction between KEAP1 and NRF2 leads to accumulation and activation of NRF2. To determine whether IL-6 disrupts the interaction between KEAP1 and NRF2, we immunoprecipitated NRF2 in the presence and absence of exogenous IL-6. IL-6 treatment increased the amount of NRF2 that was immunoprecipitated but decreased by approximately fourfold the amount of KEAP1 that was coimmunoprecipitated with NRF2 (Fig. 5*C*).

### IL-6 Signaling Links Autophagy to Antioxidant Response in β-Cells

We previously observed β-cell autophagy stimulation within 1 h of IL-6 treatment (10). To determine the kinetics of autophagy activation, we transfected INS-1 β-cells with a dual color-tagged Map1lc3 (LC3) that coalesces into puncta that are green or yellow as autophagosomes form but become red as the autophagosomes fuse with lysosomes and autophagy proceeds (14). We found that IL-6 stimulates autophagy within minutes (Fig. 6*A*), and this is accompanied by a rapid increase in LC3-II and phosphorylated p62 (phospho-p62) (Fig. 6*B* and *C*). Phosphorylation of the autophagy protein p62 at serine 351 causes it to bind to KEAP1 and to target it for degradation by autophagy (5). We found that IL-6 stimulates phosphorylation of p62 (S351) within 5 min, followed by a reduction in both phospho- and total p62 after 15 min of IL-6 treatment (Fig. 6*C*), further supporting increased autophagic flux.

We hypothesized that stimulation of p62 phosphorylation and autophagy by IL-6 may mediate IL-6-induced disruption of NRF2-KEAP1 interaction. To test this hypothesis, we used structured illumination microscopy to determine whether phospho-p62 and KEAP1 are targeted to lysosomes by IL-6. Indeed, within 15 min of IL-6 treatment, both phospho-p62 and KEAP1 colocalize with LAMP1-positive puncta (Fig. 6*D* and *E*), suggesting targeting of these proteins for degradation by IL-6-stimulated autophagy.

### Targeting of NRF2 to the Mitochondria by IL-6 Regulates Mitochondrial Function

Activation of the transcription factor NRF2 typically involves its translocation to the nucleus, where it regulates transcription of antioxidant response genes. However, no changes occurred in NRF2 target gene expression at

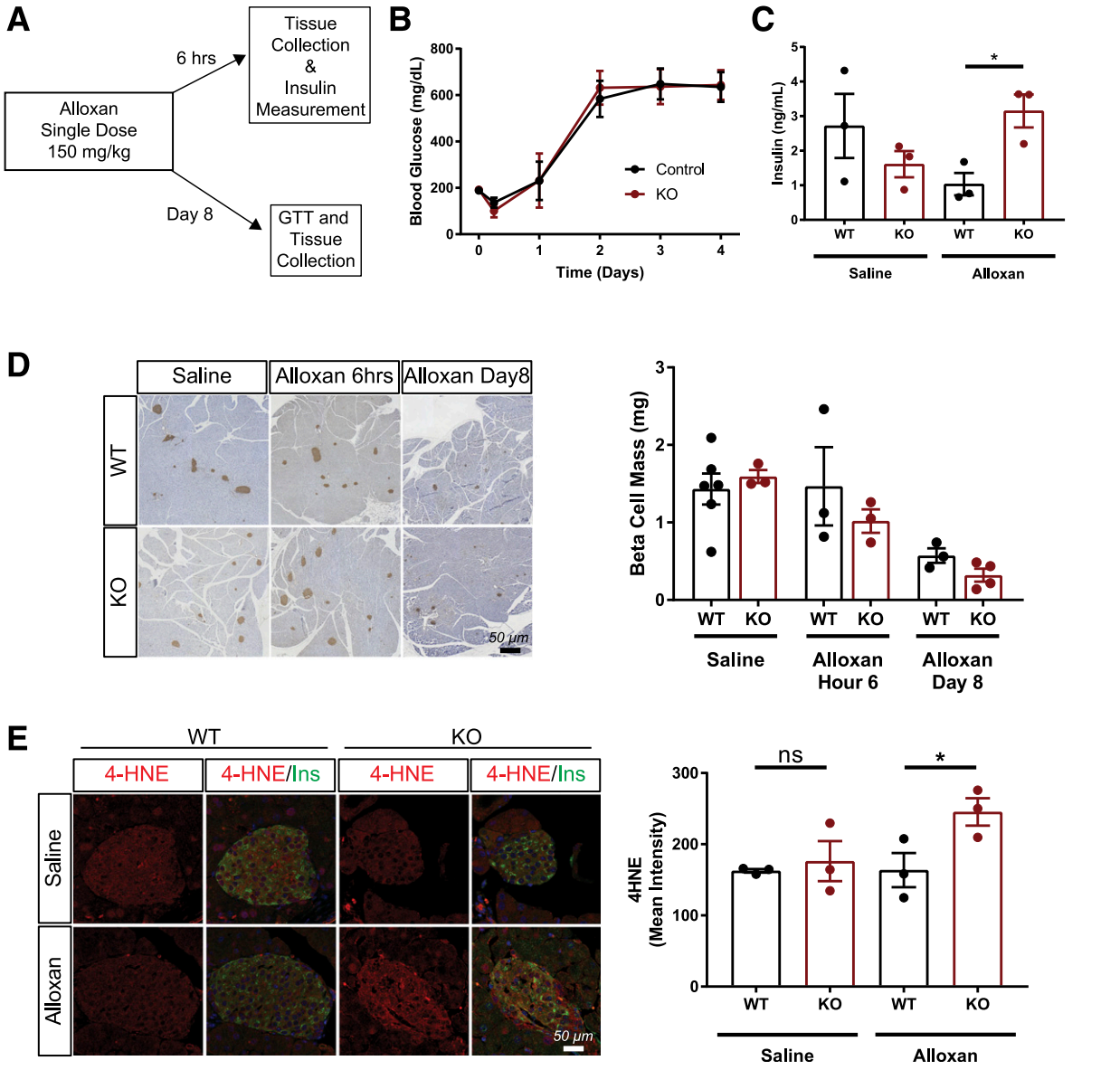


**Figure 4**—IL-6Rα$^{\Delta\beta}$ mice are more susceptible to alloxan-induced β-cell oxidative stress. *A*: Design of experiments applying alloxan treatment. *B*: Blood glucose levels in mice fed randomly were measured daily for 5 days after alloxan injection. *C*: Terminal serum insulin levels from samples collected 6 h after injection. *D*: Representative images of pancreata collected either 6 h or 8 days after alloxan treatment (left), from which β-cell mass was calculated; insulin staining appears brown. Quantification of β-cell mass is shown in the graph to the right. *E*: Representative images of pancreata collected 6 h after injection and immunostained for insulin (Ins; green) and 4-HNE (red); DAPI-stained nuclei appear blue (left). Quantification of islet 4-HNE is shown in the graph to the right. Data are mean ± SEM for 3–6 individual mice. *$P <$ 0.05. KO, knockout; ns, not significant; WT, wild type.

either the early time points at which we observed NRF2 protein accumulation in response to IL-6 treatment, or after long-term exposure to IL-6 (Fig. 7*A*). To determine whether IL-6 influences NRF2 translocation after IL-6 stimulation, we separated cytosolic, nuclear, and mitochondrial protein fractions from IL-6-treated INS-1 β-cells. Stimulation of cells by IL-6 unexpectedly led to a robust increase in mitochondrial NRF2 localization and a decrease in nuclear NRF2 levels (Fig. 7*B*).

NRF2 mitochondrial translocation has been reported in other cell types, but the mechanism and function of this translocation are not well understood (21–23). Synthetic NRF2 activators have been found to stimulate mitochondrial degradation by autophagy, a process known as mitophagy, thereby contributing to mitochondrial homeostasis (24). To determine whether IL-6 also stimulates mitophagy, we assessed translocation of the key mitophagy protein PARKIN to the mitochondria and found that IL-6 rapidly (within minutes) induces an increase in mitochondrial PARKIN levels (Fig. 7*C*). This was accompanied by an initial rapid increase in LC3 and p62 in the mitochondrial fraction. The subsequent decreases in PARKIN,

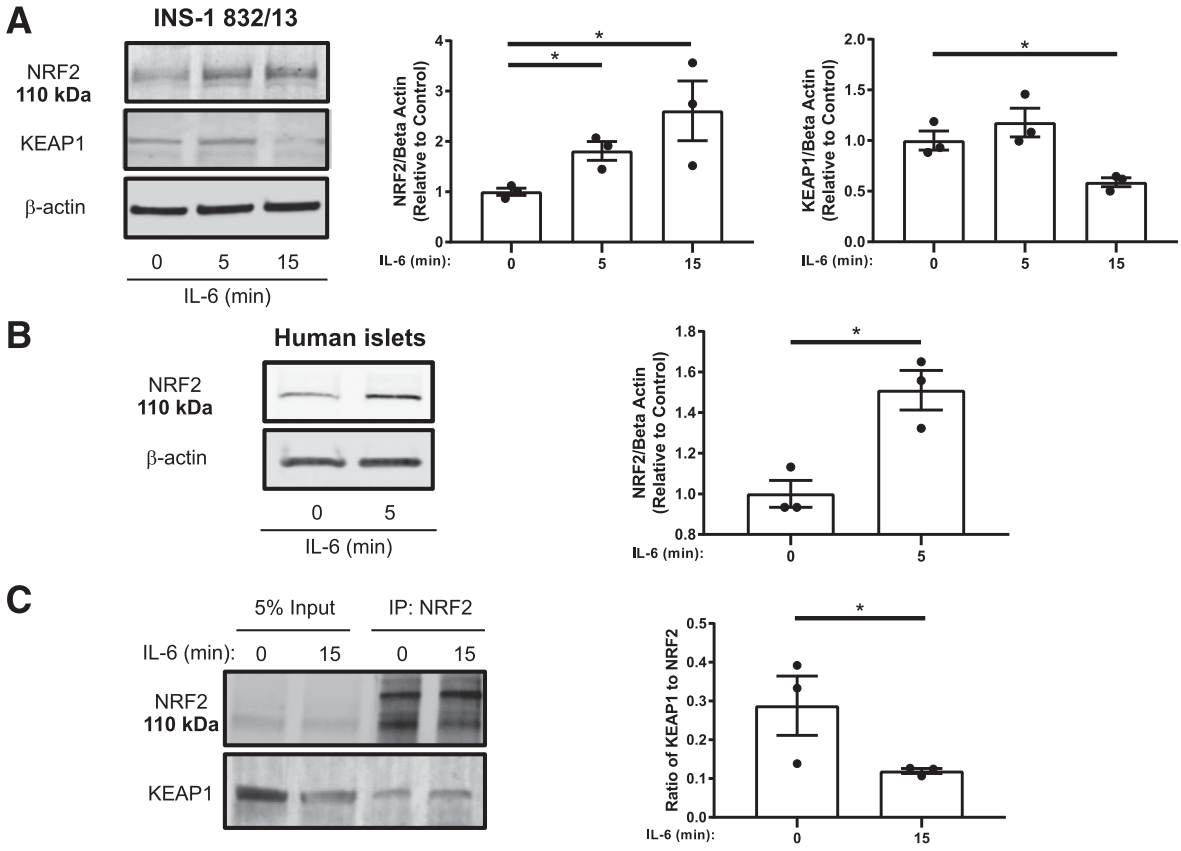


**Figure 5—** IL-6 rapidly stimulates NRF2. *A* and *B*: Representative Western blotting (*A* and *B*, left) and quantification of NRF2 (*A*, middle, and *B*, right) and KEAP1 (*A*, right) levels in response to acute treatment of INS-1 β-cells (*A*) and human islets (*B*) with IL-6. *C*: Representative Western blotting of NRF2 and KEAP1 levels in lysates from INS-1 cells treated with IL-6 immunoprecipitated (IP) with anti-NRF2 antibody (left), and quantification of coimmunoprecipitated KEAP1 relative to NRF2 (right). Data are mean ± SEM for 3 individual experiments. *$P < 0.05$.

LC3, and p62 are consistent with the progression of mitophagy (Fig. 7*C*).

Loss of mitochondrial membrane potential is also associated with the initiation of mitophagy. We imaged live cells stained with the membrane potential–dependent dye TMRM and found that IL-6 treatment results in decreased mitochondrial membrane potential (Fig. 7*D*). Both control INS-1 β-cells and those in which we had knocked down *Nrf2* by siRNA were imaged, showing an ~70% reduction in the *Nrf2* transcript and a significant decrease of NRF2 protein, which is especially evident when protein degradation by the proteasome is blocked with MG132 (Supplementary Fig. 4*A* and *B*). In both nontransfected and control siRNA–transfected cells, IL-6 treatment led to a decrease in mitochondrial membrane potential, which was blunted when *Nrf2* was knocked down (Fig. 7*D*). Also, remaining TMRM signal was clearly separated from mitochondria stained with the membrane potential–independent dye MitoTracker Green (Supplementary Fig. 4*C*), indicative of altered mitochondrial respiratory activity (25). Knockdown of *Nrf2* by siRNA abolished the IL-6-induced separation of potential-dependent TMRM and potential-independent MitoTracker (Supplementary Fig. 4*C*).

Mitochondrial fragmentation is an early event in mitophagy. cAMP levels affect the regulation of mitochondrial fusion and fission, with low cAMP levels being associated with fission (26). We found that IL-6 triggered a transient reduction of cAMP in intact mouse islets transfected with the mNeon cADDis cAMP biosensor (Fig. 7*E* and *F*). Overall, these data suggest that IL-6 orchestrates multiple events associated with the stimulation of mitophagy that likely contribute to ROS reduction in β-cells.

## DISCUSSION

IL-6 is a pleiotropic cytokine that is produced by and acts on several tissues throughout the body. This cytokine plays a well-known role in cancer cell survival, but its role in metabolism and pancreatic islet biology is more complex (27). Exercise acutely stimulates circulating IL-6 to levels that are ~50–100 times higher than those observed during resting conditions (28–30). When increased to these levels, IL-6 is associated with heightened insulin sensitivity and nutrient availability (31,32). A series of recent studies demonstrated that IL-6 signaling may play a positive role in both anti-inflammatory M2 macrophage polarization (33,34) and insulin secretion (35).

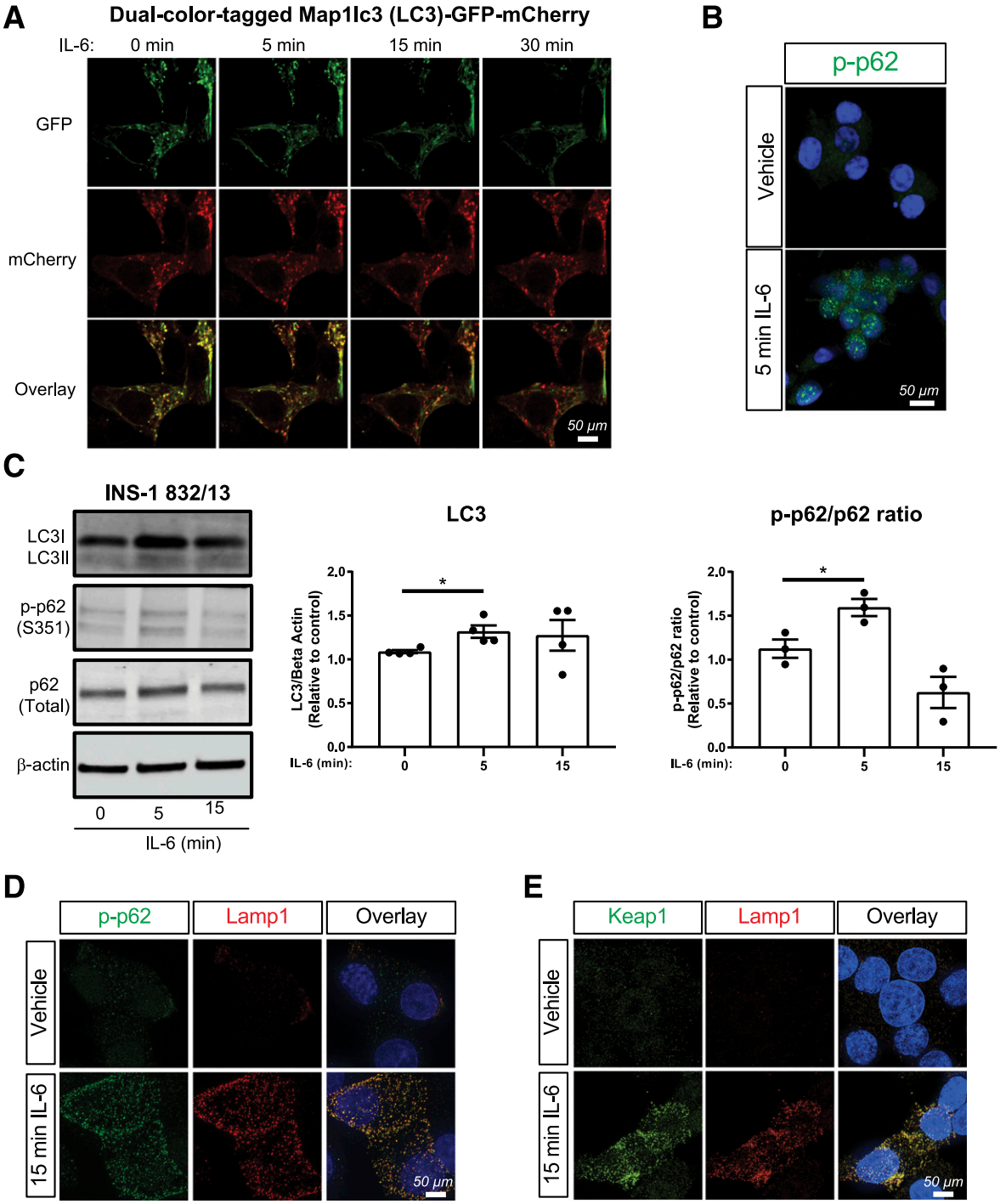


**Figure 6**—IL-6 rapidly stimulates the degradation of phospho-p62 (p-p62) and KEAP1 through autophagy. *A*: Representative snapshots from live-cell imaging of mCherry–enhanced green fluorescent protein (GFP)–LC3B in INS-1 β-cells stimulated with IL-6. *B*: Representative image showing acute stimulation of p62 phosphorylation in INS-1 cells within 5 min of IL-6 treatment. *C*: Representative Western blotting (left) and quantification of autophagy markers (LC3-II [middle] and p-p62 [right]) in INS-1 cells acutely treated with IL-6. *D*: Representative images showing colocalization of p-p62 (green) with LAMP1 (red) after 15 min of IL-6 treatment. *E*: Representative images showing colocalization of KEAP1 (green) with LAMP1 (red) after 15 min of IL-6 treatment. Data are mean ± SEM for 3 or 4 individual experiments. *$P < 0.05$.

However, circulating IL-6 is also modestly increased two- to fourfold in humans with type 1 and those with type 2 diabetes (36,37), in whom its role as a positive or negative regulator of metabolic homeostasis remains controversial (38). In fact, numerous studies have reported proinflammatory roles for IL-6 signaling and the promotion of insulin resistance in some tissues (39–42). It has been proposed that this apparent discrepancy in IL-6 action may result from cell type–specific effects, differences in acute versus chronic signaling by this cytokine, and/or differential effects of

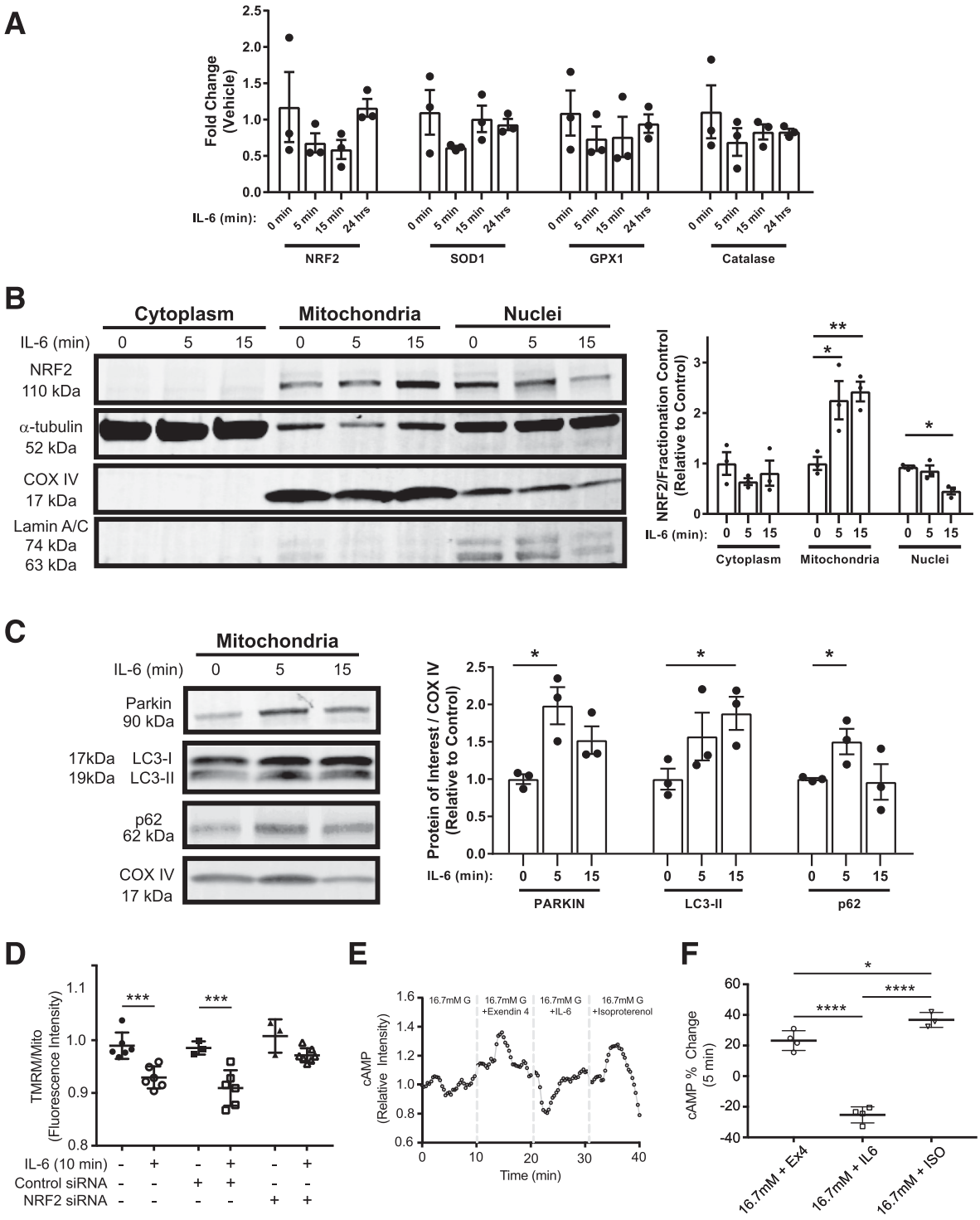


**Figure 7—**IL-6 regulates mitochondrial function through NRF2. *A*: Quantitative PCR analysis of expression of NRF2 target genes in INS-1 cells following IL-6 treatment for the indicated times. *B*: Representative Western blotting (left) and quantification (right) of NRF2 levels in fractionated INS-1 cells treated with IL-6 for the indicated times. Fractionation controls include α-tubulin (cytoplasm), cyclooxygenase (COX) IV (mitochondria), and Lamin A/C (nuclei). *C*: Representative Western blotting (left) and quantification (right) of PARKIN, p62, and LC3 levels in fractionated INS-1 cells treated with IL-6 for the indicated times. Mitochondrial fractionation control is COX IV. *D*: Mitochondrial membrane potential measurements (TMRM). Circles represent data from untransfected INS-1 cells. Squares represent data from INS-1 cells transfected with nontargeting siRNA, and triangles represent data from INS-1 cells transfected with *Nrf2* siRNA. Solid shapes represent vehicle-treated cells, and open shapes represent IL-6-treated cells. TMRM was normalized to stable MitoTracker Green (Mito) levels. *E*: Representative single-islet trace showing real-time cAMP measurements from mouse islets infected with the mNeon cADDis cAMP biosensor in the presence of glucose, exendin-4 (Ex4), IL-6, or isoproterenol (ISO). *F*: Quantification of the percentage change in cAMP relative to baseline across all replicates. Circles represent exendin-4-treated cells. Squares represent IL-6-treated cells, and triangles represent isoproterenol-treated cells. Data are mean ± SEM for 3–6 individual experiments. $^{*}P < 0.05$; $^{**}P < 0.01$; $^{***}P < 0.001$; $^{****}P < 0.0001$.

signaling through soluble and membrane-bound variants of IL6Rα (38). We recently found that increases in IL-6 had a protective effect on β-cells through the stimulation of autophagy (10). Autophagy, like IL-6, has been reported to have conflicting roles in promoting versus preventing inflammation and cell death, depending on context and duration of activation (43,44).

Here we present data supporting the hypothesis that acute IL-6 signaling in β-cells couples antioxidant response to autophagy to preserve β-cell mass under conditions of increased oxidative stress. We found that the IL-6 signaling pathway functions to reduce oxidative damage both in vitro and in vivo. β-Cell-specific knockout of IL6Rα in mice exacerbated oxidative stress, β-cell death, and hyperglycemia in response to STZ. It is worth noting, however, that in our model it is still possible that soluble IL6Rα from other cell types could be present and bind to or activate signaling through GP130 in β-cells. This could potentially diminish the effects of β-cell IL6Rα knockout, suggesting that our study may underestimate the contribution of β-cell IL-6 signaling to that response to oxidative stress.

Our data support that IL-6 protects β-cells from oxidative stress through the stimulation of autophagy and the increased accumulation of NRF2, a key regulator of the antioxidant response. We show that IL-6 stimulates translocation of NRF2 to the mitochondria and provide evidence suggesting that mitochondrial NRF2 may play a key role in the rapid response to increases in the amount of ROS in β-cells. Thus, we propose a model in which IL-6 signaling rapidly stimulates autophagy through the phosphorylation and activation of the autophagy chaperone p62, which in turn stimulates antioxidant response through phospho-p62-mediated targeting of the NRF2 inhibitor KEAP1 to the autophagosome for degradation (Fig. 8). Liberated NRF2 quickly translocates to the mitochondria, where it functions to promote redox homeostasis, similar to previous observations (45).

Mitochondria are a major source of cellular ROS. Therefore, pathways that promote mitochondrial homeostasis are critical for preventing cellular damage and death. One established mechanism for maintaining mitochondrial homeostasis is through selective degradation of dysfunctional mitochondria by mitophagy. Increases in ROS stimulate mitophagy through PINK1-mediated kinase activation of the ubiquitin ligase PARKIN (46,47). Decreases in mitochondrial membrane potential and cAMP, like those observed here in response to IL-6, are associated with the stimulation of PINK1/PARKIN-mediated mitophagy (26,48,49). Indeed, we observed that IL-6 rapidly stimulates mitochondrial translocation of PARKIN. We also showed that IL-6 induces the mitochondrial translocation of NRF2, where it has been reported to function in the modulation of respiration and to counteract ROS (21,45). Therefore, we propose that IL-6 stimulates mitochondrial turnover to reduce ROS and prevent oxidative damage and that this contributes to the restoration of homeostasis within β-cells. This protection against oxidative stress likely plays a key role in reducing apoptosis and thereby preserving β-cell mass under

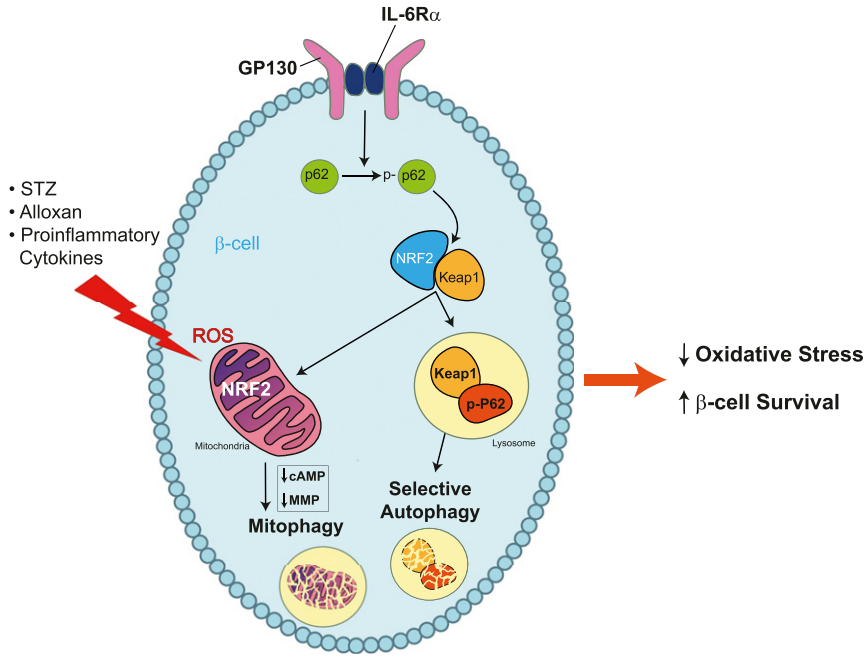


**Figure 8**—Model for IL-6-mediated oxidative stress reduction in β-cells. IL-6 signaling activates autophagy, leading to p62-mediated degradation of the antioxidant repressor KEAP1. Decreased KEAP1 allows the accumulation of NRF2, which translocates to the mitochondria, and mitophagy is stimulated to reduce ROS. Together, these events protect β-cells from oxidative stress and promote β-cell survival. MMP, mitochondrial membrane potential; p-p62, phosphorylated p62.

conditions where large amounts of ROS are generated in β-cells.

One key limitation of our study is that the in vitro activation of autophagy and the antioxidant response we observed occur so quickly that these early events would be difficult to detect in our in vivo STZ and alloxan studies. Future studies applying novel methods such as intravital microscopy could potentially be used to monitor these events in real time. This would provide valuable insight into the in vivo coupling of autophagy with antioxidant response to determine how perturbations in these pathways could contribute to diabetes development.

In conclusion, these data provide novel evidence that autophagy and antioxidant response are linked in pancreatic β-cells and that mitochondrial NRF2 may play an important role in these processes. Signaling through the IL-6 receptor quickly activates these coupled pathways, and we show that IL-6 receptor signaling is critical for reducing oxidative stress in islets, preserving β-cell mass, and protecting against STZ-induced diabetes. Therefore, we suggest that acute activation of IL-6 receptor signaling may be beneficial for protection against the development of diabetes.

**Acknowledgments.** The authors thank K. Benninger, J. Nelson, and A. Acton of the Indiana University Center for Diabetes and Metabolic Diseases Islet Core and Translation Core laboratories for expert assistance in islet isolation, metabolic characterization of mice, and insulin measurement.

**Funding.** This work was supported by the National Institute of Diabetes and Digestive and Kidney Diseases (grant nos. UC4 DK104166 to R.G.M. and K01 DK102492 to A.K.L.) and startup funds from Indiana University School of Medicine and the Herman B. Wells Center for Pediatric Research at Indiana University (to A.K.L.). This study used Diabetes Center core resources supported by the National Institute of Diabetes and Digestive and Kidney Diseases (grant no. P30 DK097512 to R.G.M.).

**Duality of Interest.** No potential conflicts of interest relevant to this article were reported.

**Author Contributions.** M.R.M., A.M.C., C.A.R., and A.K.L. designed experiments, performed research, contributed to the discussion, and wrote the manuscript. J.E.C. and E.M.A. contributed to the discussion and performed research. R.G.M. designed experiments, contributed to the discussion, and wrote the manuscript. M.R.M., A.M.C., C.A.R., J.E.C., E.M.A., R.G.M., and A.K.L. reviewed and approved the final manuscript. M.R.M. and A.K.L. are the guarantors of this work and, as such, had full access to all the data in the study and take responsibility for the integrity of the data and the accuracy of the data analysis.

**Prior Presentation.** Parts of this work were presented at ENDO 2018, Chicago, IL, 17–20 March 2018.

## References

1. Muoio DM, Newgard CB. Mechanisms of disease: molecular and metabolic mechanisms of insulin resistance and β-cell failure in type 2 diabetes. Nat Rev Mol Cell Biol 2008;9:193–205
2. Pi J, Zhang Q, Fu J, et al. ROS signaling, oxidative stress and Nrf2 in pancreatic beta-cell function. Toxicol Appl Pharmacol 2010;244:77–83
3. Robertson RP. Chronic oxidative stress as a central mechanism for glucose toxicity in pancreatic islet beta cells in diabetes. J Biol Chem 2004;279:42351–42354
4. Filomeni G, De Zio D, Cecconi F. Oxidative stress and autophagy: the clash between damage and metabolic needs. Cell Death Differ 2015;22:377–388
5. Ichimura Y, Waguri S, Sou YS, et al. Phosphorylation of p62 activates the Keap1-Nrf2 pathway during selective autophagy. Mol Cell 2013;51:618–631
6. Yagishita Y, Fukutomi T, Sugawara A, et al. Nrf2 protects pancreatic β-cells from oxidative and nitrosative stress in diabetic model mice. Diabetes 2014;63:605–618
7. Mariño G, Niso-Santano M, Baehrecke EH, Kroemer G. Self-consumption: the interplay of autophagy and apoptosis. Nat Rev Mol Cell Biol 2014;15:81–94
8. Giordano S, Darley-Usmar V, Zhang J. Autophagy as an essential cellular antioxidant pathway in neurodegenerative disease. Redox Biol 2013;2:82–90
9. Marasco MR, Linnemann AK. β-Cell autophagy in diabetes pathogenesis. Endocrinology 2018;159:2127–2141
10. Linnemann AK, Blumer J, Marasco MR, et al. Interleukin 6 protects pancreatic β cells from apoptosis by stimulation of autophagy. FASEB J 2017;31:4140–4152
11. Wruck CJ, Streetz K, Pavic G, et al. Nrf2 induces interleukin-6 (IL-6) expression via an antioxidant response element within the IL-6 promoter. J Biol Chem 2011;286:4493–4499
12. Stull ND, Breite A, McCarthy R, Tersey SA, Mirmira RG. Mouse islet of Langerhans isolation using a combination of purified collagenase and neutral protease. J Vis Exp 2012;(67). pii:4137
13. Lukowiak B, Vandewalle B, Riachy R, et al. Identification and purification of functional human β-cells by a new specific zinc-fluorescent probe. J Histochem Cytochem 2001;49:519–528
14. N'Diaye E-N, Kajihara KK, Hsieh I, Morisaki H, Debnath J, Brown EJ. PLIC proteins or ubiquilins regulate autophagy-dependent cell survival during nutrient starvation. EMBO Rep 2009;10:173–179
15. Maier B, Ogihara T, Trace AP, et al. The unique hypusine modification of eIF5A promotes islet β cell inflammation and dysfunction in mice. J Clin Invest 2010;120:2156–2170
16. Hernandez-Perez M, Chopra G, Fine J, et al. Inhibition of 12/15-lipoxygenase protects against β-cell oxidative stress and glycemic deterioration in mouse models of type 1 diabetes. Diabetes 2017;66:2875–2887
17. Eleazu CO, Eleazu KC, Chukwuma S, Essien UN. Review of the mechanism of cell death resulting from streptozotocin challenge in experimental animals, its practical use and potential risk to humans. J Diabetes Metab Disord 2013;12:60
18. Lenzen S. The mechanisms of alloxan- and streptozotocin-induced diabetes. Diabetologia 2008;51:216–226
19. Szkudelski T. The mechanism of alloxan and streptozotocin action in B cells of the rat pancreas. Physiol Res 2001;50:537–546
20. Nguyen T, Nioi P, Pickett CB. The Nrf2-antioxidant response element signaling pathway and its activation by oxidative stress. J Biol Chem 2009;284:13291–13295
21. Holmström KM, Kostov RV, Dinkova-Kostova AT. The multifaceted role of Nrf2 in mitochondrial function. Curr Opin Toxicol 2016;1:80–91
22. Strom J, Xu B, Tian X, Chen QM. Nrf2 protects mitochondrial decay by oxidative stress. FASEB J 2016;30:66–80
23. Itoh K, Ye P, Matsumiya T, Tanji K, Ozaki T. Emerging functional cross-talk between the Keap1-Nrf2 system and mitochondria. J Clin Biochem Nutr 2015;56:91–97
24. East DA, Fagiani F, Crosby J, et al. PMI: a $\Delta\Psi$m independent pharmacological regulator of mitophagy. Chem Biol 2014;21:1585–1596
25. Nguyen TT, Oh SS, Weaver D, et al. Loss of Miro1-directed mitochondrial movement results in a novel murine model for neuron disease. Proc Natl Acad Sci U S A 2014;111:E3631–E3640
26. Di Benedetto G, Gerbino A, Lefkimmiatis K. Shaping mitochondrial dynamics: the role of cAMP signalling. Biochem Biophys Res Commun 2018;500:65–74
27. Mauer J, Denson JL, Brüning JC. Versatile functions for IL-6 in metabolism and cancer. Trends Immunol 2015;36:92–101
28. Pedersen BK, Steensberg A, Fischer C, et al. Searching for the exercise factor: is IL-6 a candidate? J Muscle Res Cell Motil 2003;24:113–119
29. Pedersen BK, Steensberg A, Schjerling P. Muscle-derived interleukin-6: possible biological effects. J Physiol 2001;536:329–337
30. Febbraio MA, Pedersen BK. Muscle-derived interleukin-6: mechanisms for activation and possible biological roles. FASEB J 2002;16:1335–1347

31. Febbraio MA, Steensberg A, Keller C, et al. Glucose ingestion attenuates interleukin-6 release from contracting skeletal muscle in humans. J Physiol 2003; 549:607–612
32. Carey AL, Steinberg GR, Macaulay SL, et al. Interleukin-6 increases insulin-stimulated glucose disposal in humans and glucose uptake and fatty acid oxidation in vitro via AMP-activated protein kinase. Diabetes 2006;55:2688–2697
33. Sanmarco LM, Ponce NE, Visconti LM, et al. IL-6 promotes M2 macrophage polarization by modulating purinergic signaling and regulates the lethal release of nitric oxide during Trypanosoma cruzi infection. Biochim Biophys Acta 2017;1863:857–869
34. Mauer J, Chaurasia B, Goldau J, et al. Signaling by IL-6 promotes alternative activation of macrophages to limit endotoxemia and obesity-associated resistance to insulin. Nat Immunol 2014;15:423–430
35. Ellingsgaard H, Hauselmann I, Schuler B, et al. Interleukin-6 enhances insulin secretion by increasing glucagon-like peptide-1 secretion from L cells and alpha cells. Nat Med 2011;17:1481–1489
36. Herder C, Haastert B, Müller-Scholze S, et al. Association of systemic chemokine concentrations with impaired glucose tolerance and type 2 diabetes: results from the Cooperative Health Research in the Region of Augsburg Survey S4 (KORA S4). Diabetes 2005;54(Suppl. 2):S11–S17
37. Spranger J, Kroke A, Möhlig M, et al. Inflammatory cytokines and the risk to develop type 2 diabetes: results of the prospective population-based European Prospective Investigation into Cancer and Nutrition (EPIC)-Potsdam Study. Diabetes 2003;52:812–817
38. Fuster JJ, Walsh K. The good, the bad, and the ugly of interleukin-6 signaling. EMBO J 2014;33:1425–1427
39. Kopf M, Baumann H, Freer G, et al. Impaired immune and acute-phase responses in interleukin-6-deficient mice. Nature 1994;368:339–342
40. McLoughlin RM, Jenkins BJ, Grail D, et al. IL-6 trans-signaling via STAT3 directs T cell infiltration in acute inflammation. Proc Natl Acad Sci U S A 2005;102: 9589–9594
41. Senn JJ, Klover PJ, Nowak IA, Mooney RA. Interleukin-6 induces cellular insulin resistance in hepatocytes. Diabetes 2002;51:3391–3399
42. Yuen DYC, Dwyer RM, Matthews VB, et al. Interleukin-6 attenuates insulin-mediated increases in endothelial cell signaling but augments skeletal muscle insulin action via differential effects on tumor necrosis factor-alpha expression. Diabetes 2009;58:1086–1095
43. Netea-Maier RT, Plantinga TS, van de Veerdonk FL, Smit JW, Netea MG. Modulation of inflammation by autophagy: consequences for human disease. Autophagy 2016;12:245–260
44. Fitzwalter BE, Thorburn A. Recent insights into cell death and autophagy. FEBS J 2015;282:4279–4288
45. Dinkova-Kostova AT, Abramov AY. The emerging role of Nrf2 in mitochondrial function. Free Radic Biol Med 2015;88(Pt B):179–188
46. Frank M, Duvezin-Caubet S, Koob S, et al. Mitophagy is triggered by mild oxidative stress in a mitochondrial fission dependent manner. Biochim Biophys Acta 2012;1823:2297–2310
47. Xiao B, Goh J-Y, Xiao L, Xian H, Lim K-L, Liou Y-C. Reactive oxygen species trigger Parkin/PINK1 pathway-dependent mitophagy by inducing mitochondrial recruitment of Parkin. J Biol Chem 2017;292:16697–16708
48. Narendra D, Tanaka A, Suen D-F, Youle RJ. Parkin is recruited selectively to impaired mitochondria and promotes their autophagy. J Cell Biol 2008;183: 795–803
49. Narendra DP, Jin SM, Tanaka A, et al. PINK1 is selectively stabilized on impaired mitochondria to activate Parkin. PLoS Biol 2010;8:e1000298